Real-time, single-particle measurements of oligomers in aged ambient aerosol particles

Kerri A. Denkenberger[1], Ryan C. Moffet[1], John C. Holecek[2], Thomas P. Rebotier[1], Kimberly A. Prather[1,2*]

[1]Department of Chemistry and Biochemistry, University of California, San Diego, La Jolla, CA 92093 USA

[2]Scripps Institution of Oceanography, University of California, San Diego, La Jolla, CA 92093 USA

This supporting information section contains: 16 pages and 7 figures.

Supplemental Experimental: An in-depth discussion of the development of the A-ATOFMS is described elsewhere *(1)*. Briefly, a polonium-210 neutralizer upstream of the ATOFMS inlet is used to decrease deflection of particles with smaller vacuum aerodynamic diameters *(2)* (d_{va}<200 nm) in the ionization region. Similar to the ultrafine ATOFMS described by Su *et al*. *(3)*, particles are sampled into the A-ATOFMS through an aerodynamic lens inlet *(4,5)*, where the particles are collimated into a tight beam. The transmission bias of the aerodynamic lens system gives maximum transmission at approximately 600 nm, with the transmission efficiency dropping sharply below 200 nm and tailing off from 600-3000 nm *(1)*. Individual particles then scatter light from two mutually orthogonal 532 nm continuous wave diode-pumped solid-state lasers located 6 cm apart. For each scattering event, the photomultiplier tube detectors detect a light pulse, which is then amplified and noise-filtered before being sent to a timing circuit that records the flight time required for the particle to travel the known distance between the two scattering lasers, thus providing particle velocity. A timing circuit triggers a 266 nm pulsed Nd:YAG laser to fire when the sized particle arrives in the source region of the mass spectrometer. During SOAR, positive and negative ions generated by the LDI process were detected in this dual-polarity time-of-flight mass spectrometer with an increased data acquisition rate of approximately 6 hit particles/second *(1)*.

An in-depth discussion of the development of the automated TD system is described elsewhere *(6)*. Briefly, the heating portion of the TD consists of a 1 inch outer diameter stainless steel tube (0.0875 inch inner diameter (ID)) which is 21.8 inches long, of which 19.4 inches are wrapped by heating tape with the remainder passing through the insulation and end caps. The denuder section of the TD is 21.0 inches long with a mesh

screen (~0.75 ID) which keeps a straight passage for the particles. The total length of the TD is 46.1 inches with 3.3 inches of tubing between the heating tube and the denuding tube.

Following the observation of intense high mass negative oligomeric ions in several single-particle mass spectra, a square-wave filter was created using the mass/charge pattern of these intense oligomeric ions; using this filter, a unique search algorithm was created and run on the unheated and heated particles from August 12th and November 2-13th. For *m*/*z* -200 to -400, peaks within the allowed oligomer envelopes were assigned +1 with peaks falling outside this range -1; these values were multiplied by the normalized peak intensities and summed for each mass spectrum from *m*/*z* -200 to -400. By applying a threshold of 0.2 (95% confidence, 2 standard deviations), particles containing the oligomeric species, including those with low intensity oligomers, were identified. In this way, particles containing "random", or non-oligomeric peaks in the high mass negative ions, were eliminated. An adaptive resonance theory-based clustering method (ART-2a) was then used to classify single-particle mass spectra with a vigilance factor of 0.80, learning rate of 0.05, and 20 iterations *(7)*. By comparing the existence and intensity of ion peaks in individual single-particle mass spectra, ART-2a classifies particles into separate clusters based on their mass spectral fingerprints. For SOAR I and II, ART-2a was run separately on each study for three groups of particles: unheated total, unheated oligomer-containing, and heated oligomer-containing; the percentage of classified particles ranged from 87-94% for each of the six particle sets. All ART-2a clusters were viewed by hand to assign a general particle class based on the general mass spectral fingerprint and to verify a clear oligomeric pattern (for the oligomer-containing

ART-2a runs). Particles without a clear oligomeric pattern, including elemental carbon (EC) particles, were excluded from further analysis; this corresponded to 6-30% of the particles from the oligomer-filter results that had been classified by ART-2a. General particle classes are defined by the most dominant chemical species or possible source in an attempt to keep the naming scheme simplified; these classes do not necessarily reflect all of the species present within a particular particle type.

Supplemental Results & Discussion:

OC, amine-rich, V-rich, and EC-OC particle classes were found to contain oligomeric species. The amine-rich particle class was dominated by *m*/*z* 86 ($(C_2H_5)_2N{=}CH_2^+$); particle phase amines are formed through photooxidation and gas-particle partitioning *(8)*. V-rich particles, attributed to ship and automobile emissions, were characterized by high intensity ions at *m*/*z* 51 (V^+) and 67 (VO^+) with less intense OC and amine ion peaks; these particles are *(9)*. EC-OC particles were dominated by *m*/*z* 12 (C^+), 24 (C_2^+), and 36 (C_3^+) with less intense OC and amine ion peaks.

Particle types observed by ATOFMS during SOAR I and/or II that did not contain oligomeric species include biomass, V-rich, elemental carbon (EC), calcium-EC, ammonium-rich, metals (for example, lead-rich), and inorganic (for example, sodium-rich, calcium-rich, iron-rich), particle types typically associated with primary aerosols *(10)*. Biomass particles are dominated by m/z 39 (K^+) with less intense carbonaceous positive ions, such as *m*/*z* 27 ($C_2H_3^+$/CHN^+), 36 (C_3^+), and 37 (C_3H^+); during SOAR, the negative ions were dominated by *m*/*z* -62 (NO_3^-), -97 (HSO_4^-), and -125 ($H(NO_3)_2^-$) *(11,12)*. In the fall, the V-rich particles have less intense OC and amine ion peaks

compared to the summer V-rich particles, indicating less gas-particle partitioning of SOA, which could account for the lack of oligomers in these particles in the fall. The EC particles, typically attributed to vehicle emissions, are characterized by intense carbon cluster positive and negative ions from $C^{+/-}$ to $C_n^{+/-}$ with less intense nitrate (*m*/*z* -62 (NO_3^-)) and sulfate/phosphate (*m*/*z* -97 (HSO_4^-/$H_2PO_4^-$)) markers *(13-16)*. The mass spectra of the calcium-EC particles are similar to the EC particles with the exception of an intense *m*/*z* 40 (Ca^+) peak than suppresses the positive carbonaceous ions *(17)*. The ammonium-rich positive mass spectra are dominated by *m*/*z* 18 (NH_4^+) and 30 (NO^+) with less intense OC and amine ions; the negative ions are characterized by intense nitrate markers: *m*/*z* -62 (NO_3^-), -125 ($H(NO_3)_2^-$), and -188 (($H_2(NO_3)_3^-$) *(15,18,19)*. The metals particle type is characterized by particles containing intense ion peaks from metals such as lead (*m*/*z* 206-208 (Pb^+)) or zinc (*m*/*z* 64, 66, 68 (Zn^+)) *(20)*. Finally, the inorganic particle type is characterized by mass spectra with intense peaks due to sodium (*m*/*z* 23 (Na^+)), calcium (*m*/*z* 40 (Ca^+)), and/or iron (*m*/*z* 54, 56 (Fe^+); these spectra are mostly likely from sea-salt and dust particles *(14,21)*.

To examine the loss of semivolatile species with heating, the summer unheated oligomer-containing average mass spectra was compared to the 200°C heated oligomer-containing average mass spectra for the summer measurements. In particular, the intensities of ammonium (*m*/*z* 18(NH_4^+)), amines (*m*/*z* 58 ($C_2H_5NH{=}CH_2^+$), 86 (($(C_2H_5)_2N{=}CH_2^+$), 102 (($(C_2H_5)_3NH^+$), 118 ($(C_2H_5)_3NOH^+$)), nitrate (*m*/*z* 30 (NO^+/$CH_2{=}NH_2^+$), -46 (NO_2^-), -62 (NO_3^-), -125 ($H(NO_3)_2^-$)), and unidentified OC markers (*m*/*z* 116, 117) were observed to decreased with heating. For the summer oligomer-containing particles, Figure S7a shows the decrease in average peak area of

nitrate with increasing temperature, as well as the increase in sulfate intensity with increasing temperature. In the fall, nitrate peak area also decreases with heating for the oligomer-containing particles (Figure S7b). Due to the loss of nitrate, more electrons are available in the LDI plume to attach to the sulfate and form ions, leading to the increase in sulfate intensity.

References:

(1) Holecek, J. C.; Denkenberger, K. A.; Mayer, J. E.; Moffet, R. C.; Poon, G.; Sanchez, R.; Rebotier, T.; Furutani, H.; Su, Y.; Guazzotti, S.; Prather, K. A.; Gonin, M.; Fuhrer, K. Aircraft-ATOFMS instrument development. **2007**, *In Preparation*.

(2) DeCarlo, P. F.; Slowik, J. G.; Worsnop, D. R.; Davidovits, P.; Jimenez, J. L. Particle morphology and density characterization by combined mobility and aerodynamic diameter measurements. Part 1: Theory. *Aerosol Sci. Technol.* **2004**, *38* (12), 1185-1205.

(3) Su, Y. X.; Sipin, M. F.; Furutani, H.; Prather, K. A. Development and characterization of an aerosol time-of-flight mass spectrometer with increased detection efficiency. *Anal. Chem.* **2004**, *76* (3), 712-719.

(4) Liu, P.; Ziemann, P. J.; Kittelson, D. B.; McMurry, P. H. Generating particle beams of controlled dimensions and divergence. 1. Theory of particle motion in aerodynamic lenses and nozzle expansions. *Aerosol Sci. Technol.* **1995**, *22* (3), 293-313.

(5) Liu, P.; Ziemann, P. J.; Kittelson, D. B.; McMurry, P. H. Generating particle beams of controlled dimensions and divergence. 2. Experimental evaluation of particle motion in aerodynamic lenses and nozzle expansions. *Aerosol Sci. Technol.* **1995**, *22* (3), 314-324.

(6) Huffman, J. A., Ziemann, P.J., Jayne, J.T., Worsnop, D.R., Jimenez, J. L. A thermal denuder system for on-line coupled chemistry-volatility analysis. **2007**, *In Preparation.*

(7) Song, X. H.; Hopke, P. K.; Fergenson, D. P.; Prather, K. A. Classification of single particles analyzed by ATOFMS using an artificial neural network, ART-2A. *Anal. Chem.* **1999**, *71* (4), 860-865.

(8) Angelino, S.; Suess, D. T.; Prather, K. A. Formation of aerosol particles from reactions of secondary and tertiary alkylamines: Characterization by aerosol time-of-flight mass spectrometry. *Environ. Sci. Technol.* **2001**, *35* (15), 3130-3138.

(9) Qin, X., Shields, L.G., Toner, S.M., Prather, K.A. Single Particle Characterization in Riverside, CA during the SOAR 2005 Campaign - Part 1: Seasonal Comparisons. *Environ. Sci. Technol.* **2007**, *In preparation.*

(10) Poschl, U. Atmospheric aerosols: Composition, transformation, climate and health effects. *Angewandte Chemie-International Edition* **2005**, *44* (46), 7520-7540.

(11) Silva, P. J.; Liu, D. Y.; Noble, C. A.; Prather, K. A. Size and chemical characterization of individual particles resulting from biomass burning of local Southern California species. *Environ. Sci. Technol.* **1999**, *33* (18), 3068-3076.

(12) Guazzotti, S. A.; Suess, D. T.; Coffee, K. R.; Quinn, P. K.; Bates, T. S.; Wisthaler, A.; Hansel, A.; Ball, W. P.; Dickerson, R. R.; Neususs, C.; Crutzen, P. J.; Prather, K. A. Characterization of carbonaceous aerosols outflow from India and Arabia: Biomass/biofuel burning and fossil fuel combustion. *J. Geophys. Res.* **2003**, *108* (D15).

(13) Gross, D. S.; Galli, M. E.; Silva, P. J.; Wood, S. H.; Liu, D. Y.; Prather, K. A. Single particle characterization of automobile and diesel truck emissions in the Caldecott Tunnel. *Aerosol Sci. Technol.* **2000**, *32* (2), 152-163.

(14) Guazzotti, S. A.; Coffee, K. R.; Prather, K. A. Continuous measurements of size-resolved particle chemistry during INDOEX-Intensive Field Phase 99. *J. Geophys. Res.* **2001**, *106* (D22), 28607-28627.

(15) Pastor, S. H.; Allen, J. O.; Hughes, L. S.; Bhave, P.; Cass, G. R.; Prather, K. A. Ambient single particle analysis in Riverside, California by aerosol time-of-flight mass spectrometry during the SCOS97-NARSTO. *Atmos. Environ.* **2003**, *37*, S239-S258.

(16) Moffet, R. C.; Shields, L. G.; Bernsten, J.; Devlin, R. B.; Prather, K. A. Characterization of an ambient coarse particle concentrator used for human exposure studies: Aerosol size distributions, chemical composition, and concentration enrichment. *Aerosol Sci. Technol.* **2004**, *38* (11), 1123-1137.

(17) Spencer, M. T.; Shields, L. G.; Sodeman, D. A.; Toner, S. M.; Prather, K. A. Comparison of oil and fuel particle chemical signatures with particle emissions from heavy and light duty vehicles. *Atmos. Environ.* **2006**, *40* (27), 5224-5235.

(18) Hughes, L. S.; Allen, J. O.; Kleeman, M. J.; Johnson, R. J.; Cass, G. R.; Gross, D. S.; Gard, E. E.; Galli, M. E.; Morrical, B. D.; Fergenson, D. P.; Dienes, T.; Noble, C. A.; Silva, P. J.; Prather, K. A. Size and composition distribution of atmospheric particles in southern California. *Environ. Sci. Technol.* **1999**, *33* (20), 3506-3515.

(19) Liu, D. Y.; Prather, K. A.; Hering, S. V. Variations in the size and chemical composition of nitrate-containing particles in Riverside, CA. *Aerosol Sci. Technol.* **2000**, *33* (1-2), 71-86.

(20) Liu, D. Y.; Wenzel, R. J.; Prather, K. A. Aerosol time-of-flight mass spectrometry during the Atlanta Supersite Experiment: 1. Measurements. *J. Geophys. Res.* **2003**, *108* (D7).

(21) Silva, P. J.; Carlin, R. A.; Prather, K. A. Single particle analysis of suspended soil dust from Southern California. *Atmos. Environ.* **2000**, *34* (11), 1811-1820.

(22) Spencer, M. T.; Prather, K. A. Using ATOFMS to determine OC/EC mass fractions in particles. *Aerosol Sci. Technol.* **2006**, *40* (8), 585-594.

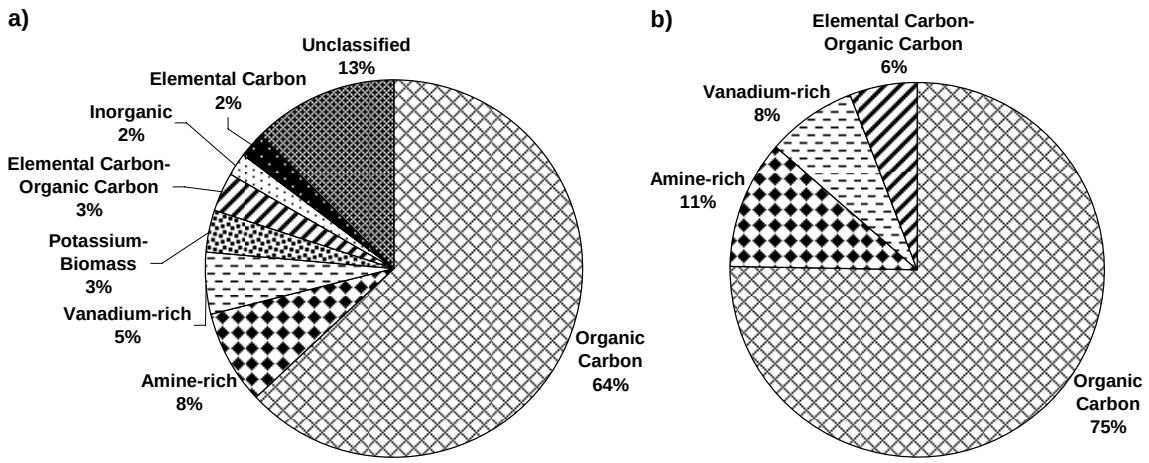

Figure S1. Relative contributions of different particle types during the summer for a) all unheated particles and b) unheated oligomer-containing particles. Particles not containing the oligomeric pattern are not included in part b); thus, no "unclassified" particles are shown.

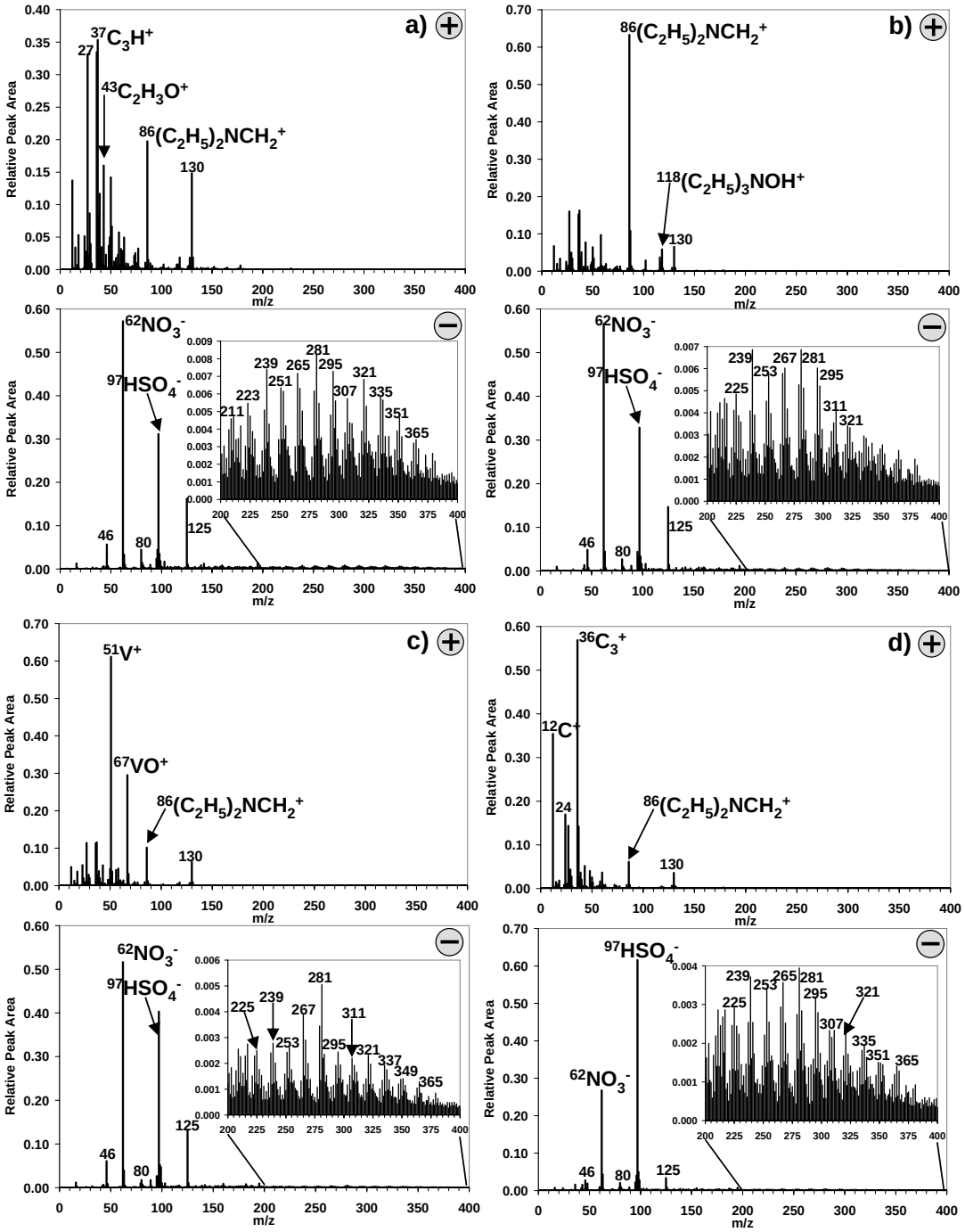

Figure S2. Average positive and negative mass spectra of the four oligomer-containing summer unheated particle types: a) OC, b) amine-rich, c) V-rich, and d) EC-OC.

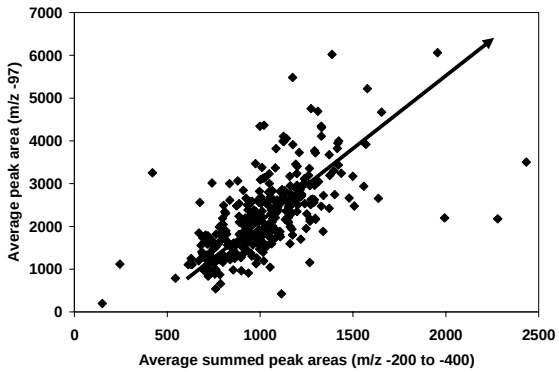

Figure S3. Correlation between oligomer intensity (m/z -200 to -400) and sulfate intensity (m/z -97) for the summer unheated oligomer-containing particles.

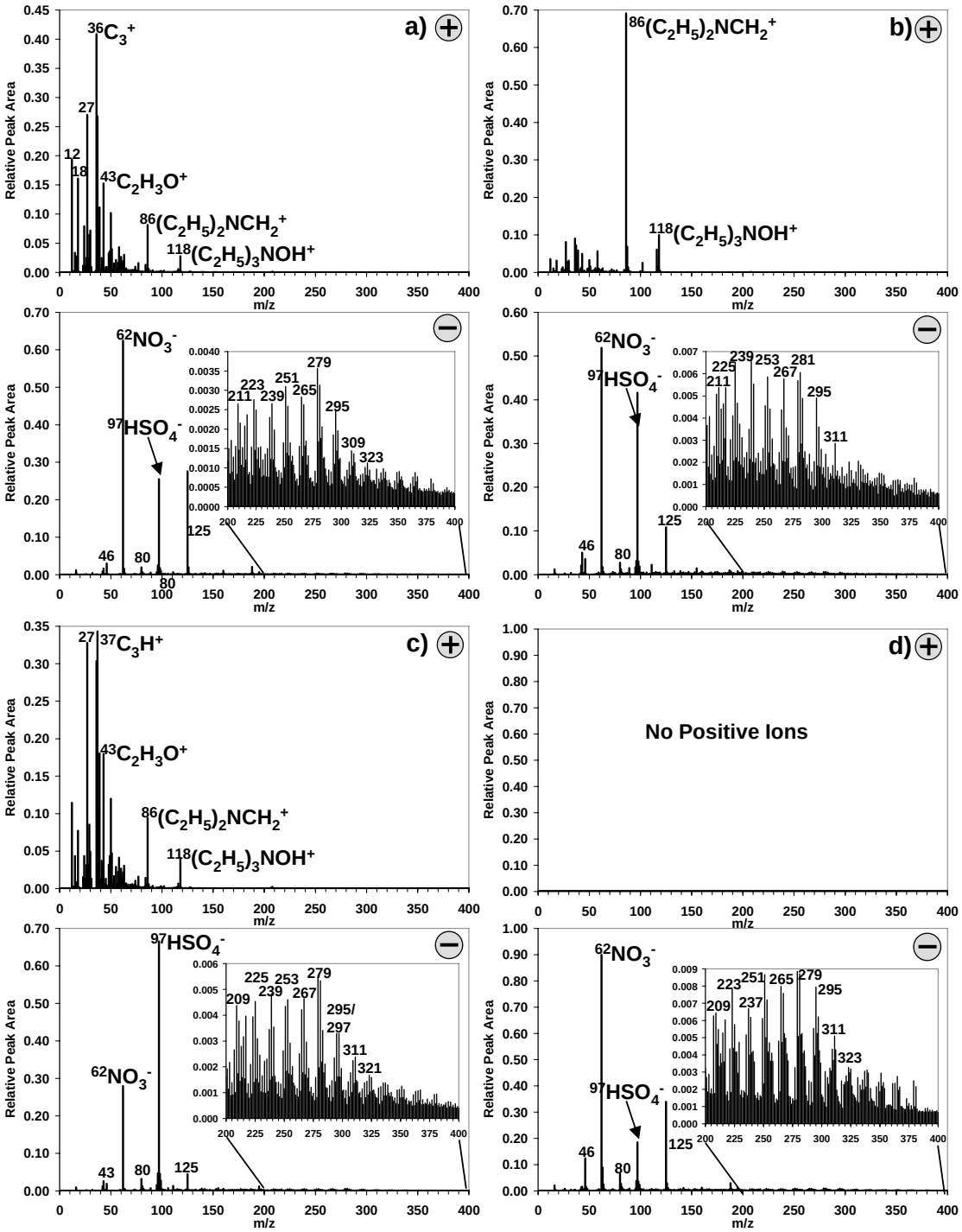

Supplementary Figure S4. Average positive and negative mass spectra of the four oligomer-containing fall unheated particle types: a) EC-OC, b) amine-rich, c) OC, and d) nitrate-sulfate, which contain only negative ions due to instrumental issues.

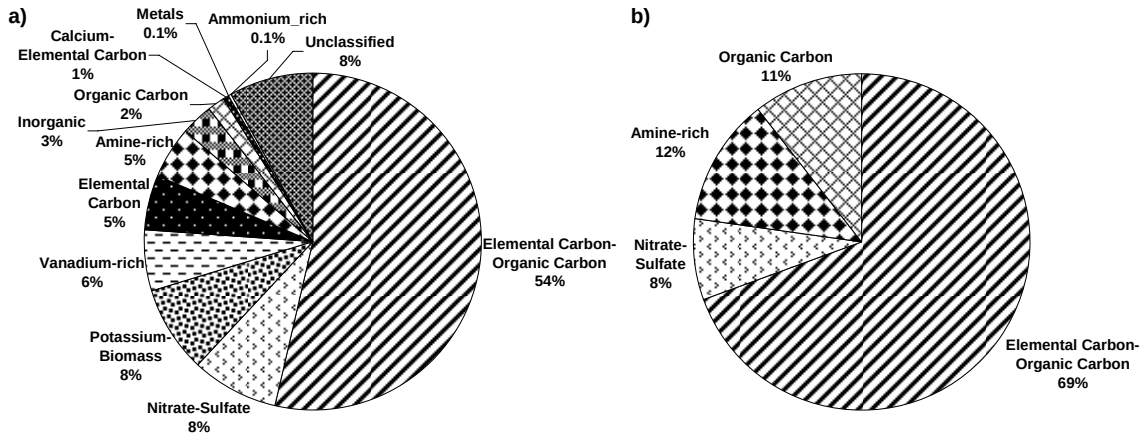

Figure S5. Relative contributions of different particle types during the fall for a) all unheated particles and b) unheated oligomer-containing particles. Particles not containing the oligomeric pattern are not included in part b); thus, no "unclassified" particles are shown.

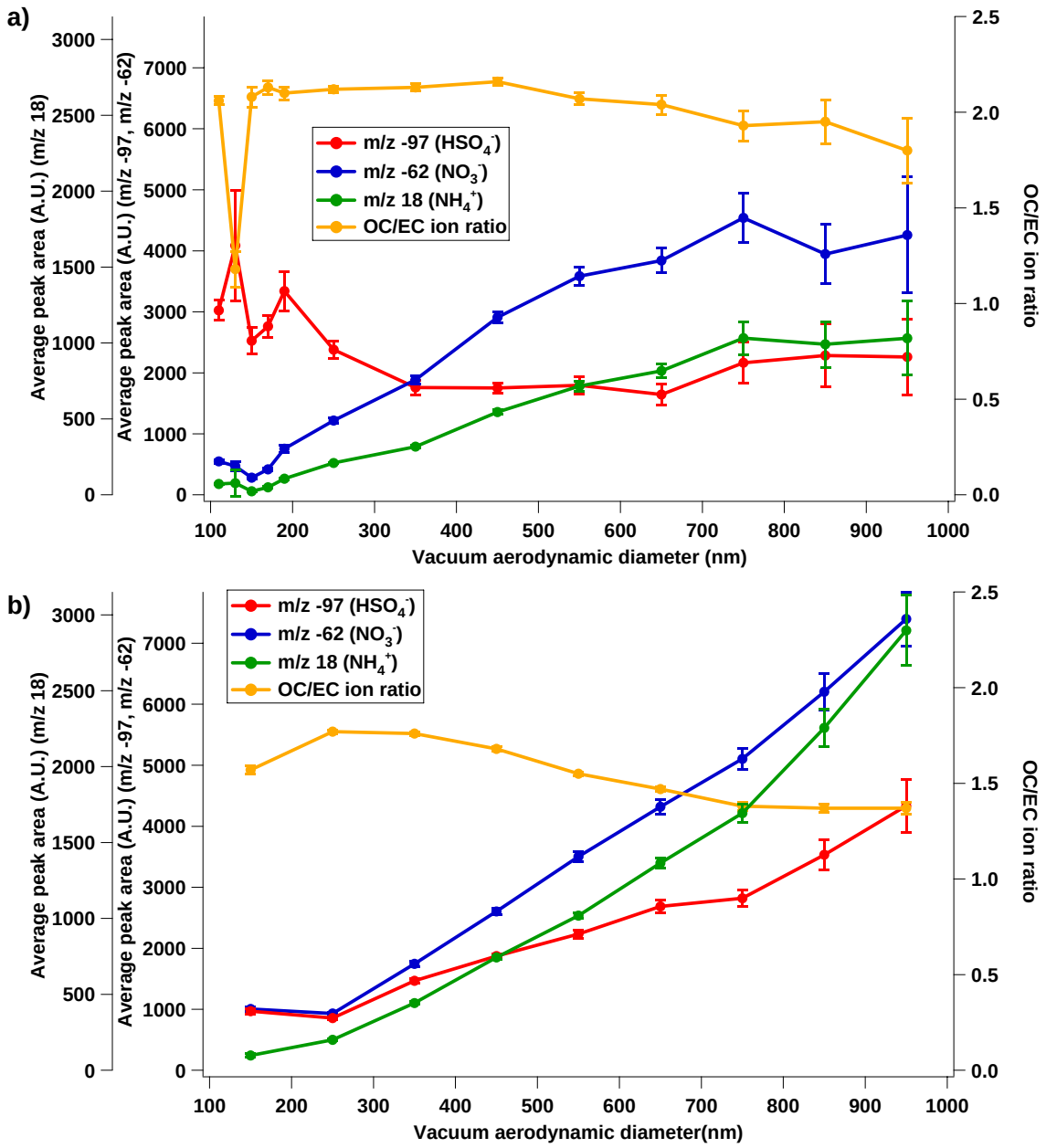

Figure S6. OC/EC ion ratios and average peak areas of *m/z* 18 (NH_4^+), -62 (NO_3^-), and -97 (HSO_4^-) versus vacuum aerodynamic diameter (nm) for the a) summer and b) fall unheated oligomer-containing particles. The OC/EC ion ratio, calculated using the method by Spencer *et al*. *(22)*, is relatively constant versus particle diameter (d_{va}), showing that these oligomer-containing particles possess relatively similar amounts of OC with respect to EC; when all particles, including those not containing oligomers, were

considered in considered in the calculation of the OC/EC ion ratio, the OC/EC ion ratio decreased for particles less than 200 nm in diameter, as shown by Spencer *et al*. *(22)*.

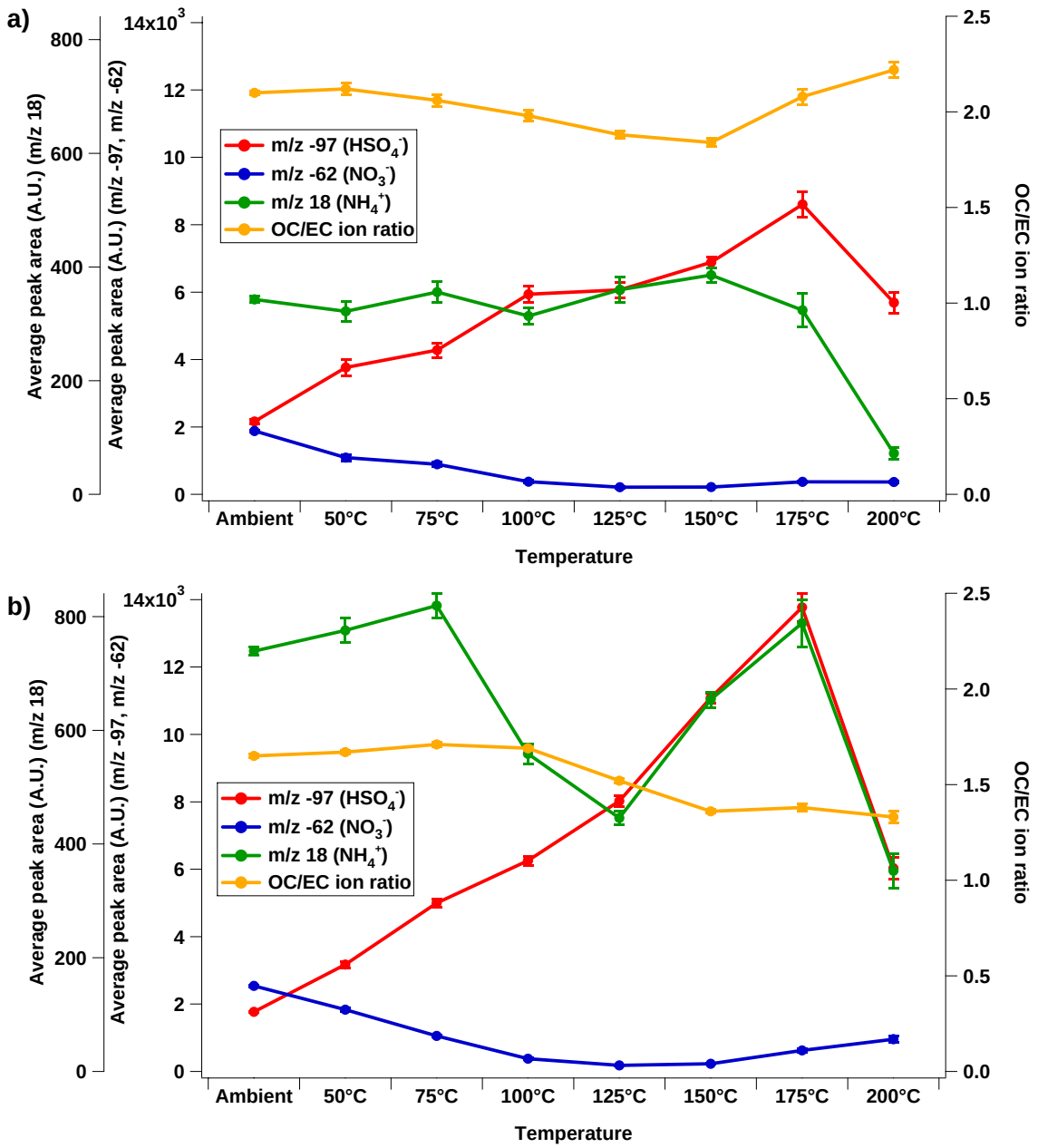

Figure S7. OC/EC ion ratios and average peak areas of *m/z* 18 (NH_4^+), -62 (NO_3^-), and -97 (HSO_4^-) versus TD temperature for the a) summer and b) fall oligomer-containing particles.